Genetic Algorithm Assisted Parametric Design of Splitting Inductance in High Frequency GaN-based Dual Active Bridge Converter

Wang, Chang; Zsurzsan, Tiberiu Gabriel; Zhang, Zhe

Published in:
IEEE Transactions on Industrial Electronics

Link to article, DOI:
10.1109/TIE.2021.3102398

Publication date:
2022

Document Version
Peer reviewed version

Genetic Algorithm Assisted Parametric Design of Splitting Inductance in High Frequency GaN-based Dual Active Bridge Converter

Chang Wang, *Student Member*, *IEEE*, Gabriel Zsurzsan, Member, *IEEE,*
and Zhe Zhang, *Senior Member, IEEE*

Abstract*—Splitting and placing interfacing inductance on both sides of the transformer has been proven to be an effective method, which extends the zero-voltage switching (ZVS) region for all the switching devices in the dual active bridge (DAB) converter. With the trend towards operating in higher frequency, achieving higher power density and higher efficiency, the converter model becomes more complex due to the non-negligible parasitic components that brings new challenges to DAB converter design. Traditional analytical methods have become hardly to imitate the proposed converter neither easily or precisely. Thus, artificial intelligence (AI) techniques are able to be utilized to assist the design process. When considering the converter system as a gray-box model, the metaheuristic algorithm can be implemented for the targeted design inside such gray-box. In this paper, a genetic algorithm (GA) is employed in the DAB converter parametric design with an explicit fitness desire and helps in discovering the high frequency oscillation (HFO) problem. Consequently, the splitting inductance tuning method is proposed for eliminating the HFO problem and minimizing inductors' loss. The methodology of implementing GA into converter parametric design and the proposed splitting inductance tuning method are introduced and verified with a 1 MHz Gallium Nitride high-electron-mobility transistor (GaN HEMT) based DAB converter prototype. The comparison experimental results prove the effectiveness of the splitting inductance tuning method and achieve 4% efficiency enhancement with 200W power delivering.

***Index Terms*—Dual active bridge, splitting inductance tuning method, zero-voltage switching, gray-box model, artificial intelligence, genetic algorithm**

I. Introduction

Substantial research has been performed for dual active bridge (DAB) converters since it was proposed in [1]. Through decades of development, the DAB converter is widely employed in various industrial applications such as electric vehicles, fuel cell power conversion, renewable energy storage system, etc [2][3].With the desire for higher efficiency and higher power density power converters, the operating frequency is usually increased to megahertz (MHz) range [4][5]. Consequently, soft-switching has become more important to high frequency DAB converters due to the increase of switching loss. There are various DAB modulation schemes, e.g. single-phase-shift (SPS), dual-phase-shift (DPS), triple-phase-shift (TPS) and multi-phase-shift (MPS) are different modulation strategies. Comparing DPS, TPS and MPS with SPS, the duty ratio as an additional degree of freedom is adopted mainly for shaping the inductor current to fulfil zero-voltage switching (ZVS) condition. Most analysis of ZVS typically depends on the resonance between the inductance along the ac link and switch output capacitance C_{oss} while the resonant loop also varies under different modulation strategies [6]. However, under high operating frequency, the transformer's parasitic capacitances become non-negligible, which can cause the current resonance and the narrowing of the ZVS region [7]. To mitigate the current resonance, the approach of distributing the external inductance on both sides of the transformer is introduced and analyzed in [2]. With the consideration of more parasitics, the converter model becomes more complicated and makes it harder to derive a precise analytical model. Thus, the whole system can be regarded as a gray-box. To obtain the targeted design inside the gray box more efficiently, the use of artificial intelligence (AI) becomes a promising choice.

AI technology has been expanding rapidly in the present era, aiming to utilize the massive computing power to facilitate systems with human-like intelligence. With human-like learning and reasoning ability, AI can be involved in numerous industrial tasks assisting in classification, optimization, regression and data exploration [8]. Power electronics can benefit from AI in various projects, e.g., active damping design [9], multi-objective optimization of transformer [10][11], maximum power point tracking (MPPT) control for photovoltaic systems [12], system reliability design [13], etc. Among them, the genetic algorithm (GA) and particle swarm optimization (PSO) are the most commonly used methods for optimizing power electronics converters [8]. Comparing with other methods like PSO or non-linear least squares, GA is effective in simple objective optimization and relatively reliable in searching for the global optimum rather than local optimum, however, less effective in solving multi-objective problems.

In this paper, a GA is employed in the DAB converter

C. Wang, G. Zsurzsan, and Z. Zhang are with the Department of Electrical Engineering, Technical University of Denmark, Kgs. Lyngby 2800, Denmark (e-mail: chawa@elektro.dtu.dk; tgzsur@elektro.dtu.dk; zz@elektro.dtu.dk). Corresponding author: Zhe Zhang.

Supporting materials such as corresponding Python code can be found in GitHub: https://github.com/JeromeWang123/Chang_GA_DAB

parametric design for inductors' loss optimization. With an explicit fitness desire for converter design, the GA takes the place of complicated mathematical derivation and provides us with a targeted parametric design through the calculation inside the gray-box model.

According to the GA assisted optimization result, the high frequency oscillation (HFO) problem is discovered in this case. As mentioned in previous literature [14], the HFO problem is tricky and can be effectively solved by paralleling the capacitors to the switching device to slow down the switching speed. However, which is against to the high frequency trend. Consequently, the splitting inductance tuning method is proposed to solve the HFO problem. A 1 MHz GaN-based DAB converter prototype is built and the experimental comparison result validates the design.

II. Specification of DAB Converter

The topology of the DAB converter including the transformer parasitic capacitances C_{p1} and C_{p2} is shown in Fig. 1. The L_{k1} and L_{k2} represent the leakage inductances of the transformer while the L_{e1} and L_{e2} are the external inductances splitting into the high-voltage (HV) side and low-voltage (LV) side of the transformer. To keep the equivalent inductance referred to the primary side of the transformer L_e unchanged, the two external inductances have the following relation,

$$L_{e1} + N^2 L_{e2} = L_e \quad (1)$$

Throughout theoretical analysis and simulations in [2], it is revealed that the existence of C_{p1} and C_{p2} leads to a non-sinusoidal switching-node voltage V_{ac1}. The increase of the high-voltage side external inductance L_{e1} forms a quasi-sinusoidal V_{ac1} which further reduces the minimum dead time to achieve ZVS. The specifications of the constructed experimental prototype are listed in TABLE I, with the parameters extracted as shown in TABLE II.

Those constraint regions from specifications and ZVS analysis are not enough to specify the inductances. With different combinations of inductances value, the commutation loop of the converter and its operating conditions can still be different with parasitics involved. As the system efficiency is an important criterion to evaluate the performance and loss of both inductors are the main difference while keeping other parameters consistent. The minimized inductors' loss design should be further investigated to specify the inductance value within the given design region.

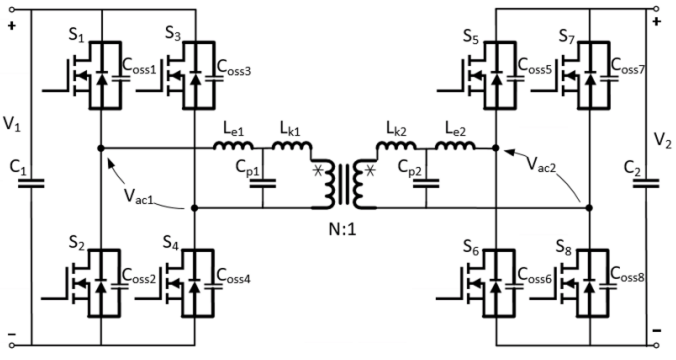

Fig. 1.Topology of the DAB Converter

TABLE I.Specifications of the DAB Prototype

	Description	Parameter
Specifications	Switching frequency	1 MHz
	DC voltage on the HV side	200 V
	DC voltage on the LV side	50 V
	Rated output power	200 W
Power semiconductor	Switches on the HV side	GS66502B
	Switches on the LV side	EPC2016C
Transformer	Core's material, type, size and turns ratio	Hitachi Metals ML91S, 2×EE-21.8-11.4-15.8, 8:2

TABLE II. Parameters Used in Calculations and Simulation

L_M	646 μH	N	4
L_{k1}	1300 nH	L_{k2}	81 nH
C_{p1}	28 pF	C_{p2}	430 pF
L_{e1}	0 μH-24 μH	L_{e2}	(24 μH-L_{e1})/N^2

III. Implementation of Genetic Algorithm into Parametric Design

A. Inductors' Loss Identification and Simplification

As is mentioned in the previous section, within the design range, the external inductances must be specified in order to obtain the minimized loss design.

Since the interfacing inductors of the DAB converter is a pure ac inductor, with the switching frequency f_s of 1 MHz operating, the inductor ac resistance R_{ac} and current root-mean-square (RMS) value I_{RMS} are used to calculate the copper loss. The current flowing through the inductors is of quasi-trapezoidal shape in the time domain and can be converted to the frequency domain using Fast Fourier Transform (FFT). With different harmonic current RMS value and the ac resistance to dc resistance ratios under different harmonic frequencies, the copper loss P_{cu} can be calculated in the following equation, where the ρ_w represents the resistivity of the conductor, the l_w represents the total length of the conductor and A_w represents the cross-section of the conductor. The core loss is kept equal with choosing same core shape, magnetic material and same peak flux density, thus, not included into the optimization objective.

$$P_{cu} = \sum_{k=1}^{n} I_{RMS}(kf_s)^2 R_{ac}(kf_s)$$
$$= \sum_{k=1}^{n} \rho_w \frac{l_w}{A_w} I_{RMS}(kf_s)^2 \frac{R_{ac}}{R_{dc}}(kf_s) \quad (2)$$

The simplified computation can be made for the inductor copper loss of each harmonic current, where the N is the number of turns and the MLT is the mean length of a single turn,

$$P_{cu} = \rho_w \frac{l_w}{A_w} I_{RMS}^2 \frac{R_{ac}}{R_{dc}} = \frac{\rho_w N\ MLT\ I_{RMS}^2}{A_w} \frac{R_{ac}}{R_{dc}} \quad (3)$$

Given a gapped core, the inductance L is defined as:

$$L = \frac{\mu_{\text{eff}}\mu_0 N^2 A_{\text{e}}}{l_{\text{e}}} \tag{4}$$

where the μ_{eff} is the effective relative permeability, μ_0 is the vacuum permeability, A_{e} is the effective magnetic cross section and l_{e} is the effective magnetic path length of the core.

Substituting (3) into (4) obtains:

$$\frac{P_{\text{cu}}}{L} = \frac{\rho_{\text{w}} MLT I_{\text{RMS}}^2 l_{\text{e}}}{A_{\text{w}}\mu_{\text{eff}}\mu_0 N A_{\text{e}}}\frac{R_{\text{ac}}}{R_{\text{dc}}} \tag{5}$$

According to Ampere's law, the maximum flux density B_{max} can be calculated,

$$B_{\text{max}} = \mu_{\text{eff}}\mu_0 H_{\text{max}} = \frac{\mu_{\text{eff}}\mu_0 N\hat{I}}{l_{\text{e}}} \tag{6}$$

where H_{max} is the maximum magnetic field intensity and $\hat{\imath}$ is the inductor peak current. It can be reorganized as,

$$N = \frac{B_{\text{max}} l_{\text{e}}}{\mu_{\text{eff}}\mu_0 \hat{I}} \tag{7}$$

Substituting (7) into (5) gets:

$$P_{\text{cu}} = \frac{\rho_{\text{w}} MLT I_{\text{RMS}}^2 \hat{I} L}{A_{\text{w}} B_{\text{max}} A_{\text{e}}}\frac{R_{\text{ac}}}{R_{\text{dc}}} \tag{8}$$

Assuming the core window area A_{win} utilization ratio U_{space} is around 20%, the conductor cross-section area A_{w} can then be expressed as,

$$A_{\text{w}} = \frac{U_{\text{space}} A_{\text{win}}}{N} \tag{9}$$

Substituting (9) into (8) obtains:

$$P_{\text{cu}} = \frac{\rho_{\text{w}} MLT I_{\text{RMS}}^2 \hat{I} L N}{U_{\text{space}} A_{\text{win}} B_{\text{max}} A_{\text{e}}}\frac{R_{\text{ac}}}{R_{\text{dc}}} \tag{10}$$

For the air-gapped core, the effective relative permeability is,

$$\mu_{\text{eff}} = \frac{1}{\frac{1}{\mu_{\text{r}}} + \frac{1}{l_{\text{e}}/g}} \approx \frac{l_{\text{e}}}{g} \tag{11}$$

where g is the gap length and the μ_{r} is the relative permeability of the magnetic material which can be neglected due to the small value compare to the l_e/g.

Substituting (11) into (4) and (5) gets:

$$L = \frac{\mu_0 N^2 A_{\text{e}}}{g} \tag{12}$$

$$B_{\text{max}} = \frac{\mu_0 N\hat{I}}{g} \tag{13}$$

Combining (12) with (13) obtains:

$$N = \frac{L\hat{I}}{B_{\text{max}} A_{\text{e}}}, g = \frac{\mu_0 L\hat{I}^2}{B_{\text{max}}^2 A_{\text{e}}} \tag{14}$$

Substituting (14) into (10) gives:

$$P_{\text{cu}} = \frac{\rho_{\text{w}} MLT I_{\text{RMS}}^2 \hat{I}^2 L^2}{U_{\text{space}} A_{\text{win}} B_{\text{max}}^2 A_{\text{e}}^2}\frac{R_{\text{ac}}}{R_{\text{dc}}} \tag{15}$$

With the given core size E22/6/16 listed in TABLE I, B_{max}=*50 mT* for ML91s magnetic material, and the $R_{\text{ac}}/R_{\text{dc}}$=*30* empirically [4] due to the similar design method and manufacturing procedure. The copper loss can then be expressed as a function of inductor ac current RMS value, peak value, and the inductance.

$$\begin{aligned} P_{\text{cu}} &= \frac{1.7e-8\cdot 65.2\text{e}-3\cdot I_{\text{RMS}}^2 \hat{I}^2 L^2}{20\%\cdot 37.76e-6\cdot (50e-3)^2\cdot (79e-6)^2}30 \\ &= 2.82e8\cdot I_{\text{RMS}}^2 \hat{I}^2 L^2 \end{aligned} \tag{16}$$

B. Gray-box model of the DAB Converter

The traditional method for deriving the inductor current is to set up the converter mathematical model and solve it using the algebraic method as shown in Fig. 2. There are several approaches to modelling the DAB converter: 1) a simplified reduced-order model [15]; 2) a full-order discrete-time model [16]; and 3) a full-order continuous-time average model [17]. It's obvious that with the higher order model and with continuous-time modelling, the accuracy will be higher compared to the discrete-time model of reduced order. However, there are still plenty of assumptions and simplifications before modelling of the DAB converter. E.g., neglecting the equivalent series resistance (ESR) of different passive components to reduce the sixth-order model to a third-order model [17] or neglecting the parasitic capacitance of the transformer [18] are two prevalent methods. However, the accuracy of the model will gradually decay with operating at higher frequency since more parasitic components are engaged into the operation.

The modelling of the DAB transformer and inductor can be extracted by the impedance curve fitting method proposed in [7]. With the impedance measurement of the constructed prototype, the accurate parasitic value of the transformer and inductor model can be obtained, where the parasitic capacitances of the transformer are vital to the transformer current shape since they form the resonance with the inductors of DAB converter. Furthermore, high-frequency resonant current will flow into the circuit worsening the switches' soft-switching performance and generating extra loss on the high-frequency ac resistance of the inductors and transformer. With the development of MOSFET modelling [19] and GaN HEMTs modelling [20], accurate power switch models can be derived. Temperature effects on the conductivity and threshold parameters can be incorporated into the switch model. The capacitance of the power switch is not constant but expressed as a function of the gate, drain and source voltage V_{G}, V_{D} and V_{S} as shown in Fig. 3. With the above modelling method implemented on the DAB converter, the converter becomes a complicated high-order system, which makes it even more difficult to resolve the mathematical expression of the inductor current. The relationship between the given specifications and the desired inductor current is no longer as simple as a linear function, but is now a matrix of the selected switch type including the parasitic values, the transformer parasitic value and the inductor parasitic value. Inside the elements of the matrix, the value is also a matrix of the thermal performance, voltage-based capacitance source and so on. Thus, the system can be regarded as a gray-box model with high-order complexity as shown in Fig. 4.

Then, the gray-box model of the DAB converter can be built up in Simulation Program with Integrated Circuit Emphasis (SPICE) based on the given specification, transformer parasitic and manufacturer-provided switch library. With the simulated circuit, the required value in (16) of each current harmonic can be easily obtained with FFT analysis of the steady-state current waveform in the time domain. Note that even with parasitics involved, the power is kept constant with little variance in simulations, which is 185W±1.6% in this case.

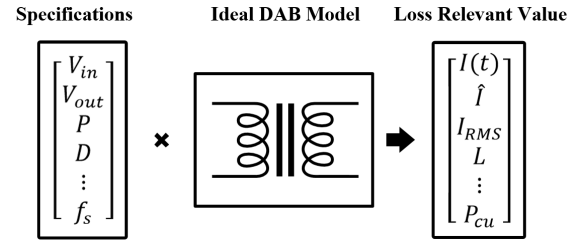

Fig. 2.Traditional Modelling Method

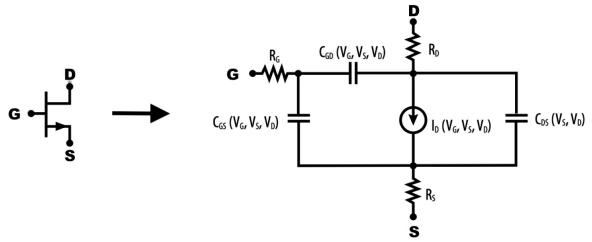

Fig. 3.Applied Power Switch Model

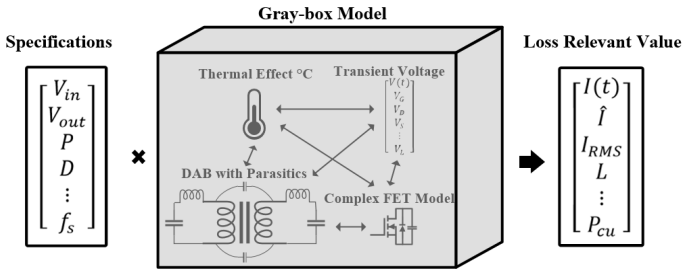

Fig. 4.Gray-box Modelling Method

C. Implementing the Genetic Algorithm

Early researches have constructed the theoretical framework of the GA [21][22], where the concept initially stemmed from the population genetics and evolution theory. It's an iteration procedure with unchanged population size. Each population is generated mainly by the candidates selected from the previous population, the combination of those candidates which is called cross-over, and the candidates of mutation after the cross-over which is learnt from the chromosomal alteration from biology. The initial generation is often chosen by random within the given range. The choice of the candidates from the previous population depends on the desired fitness value, where the one with better fitness value tends to survive and be selected into the next generation. The mutation of the population contributes to the avoiding of the local optimal solution because it draws attention to other areas within the given range and gives chances to the unlucky ones that are not initially generated in the previous generations. The implementation of the GA for this case is described as the following sequence,

a) Generating the initial population $\boldsymbol{L}$ with the population size N = 23 according to the computing power and parallel processing ability of the applied facility. The initial population is a series of the random HV inductance value within the design range described in the previous section. And the inductance range is divided into 1024 sections, where 10-bits binary numbers are encoded for each decimal value.

$$L_{e1} + N^2 L_{e2} = 24\,uH$$
$$0\,uH < L_{e1} < 24\,uH\ (0\,nH < L_{e2} < 1.5\,uH)$$

b) Squeezing the generated population into the constructed gray-box model, which is invoking SPICE model built with LTspice with the initialized inductance value $L \in \boldsymbol{L}$ for circuit simulation to get the required inductor current RMS values and peak values

c) The Fitness value F is defined as the fourth power of the difference between the maximum copper loss value among the present populations and the copper loss of each individual of the population. The copper loss is computed by using (16), which is also the optimization target in this case. The fourth power of the difference makes the converging faster by magnifying the difference within each population but slightly increases the chance of obtaining the local optimum

$$F = \left(\max_N P_{\mathrm{cu}} - P_{\mathrm{cu}}\right)^4$$

d) Selecting the individuals from the population with the possibility P, where the P is defined as the percentage of each fitness value over the sum of the fitness values. The selection is carried out with the replacement, thus, the population size is unchanged

$$P = \frac{F}{\sum_1^N F}$$

e) Operating the Cross-over of the chosen individuals (inductances) from step d), which are encoded with the 10-bits binary numbers imitating the biological DNA. The parents from the population are chosen randomly and the cross-over bits are selected also randomly. The cross-over will then be operated by combining the selected cross-over bits from parent 1 and the others from parent 2. The cross-over rate is set to be 0.8 and Fig. 5 shows the schematic of the cross-over process. Usually, the cross-over rate is set to be around 0.5 ~ 1

f) Enabling the mutation of children's DNA moderately with mutation rate M = 0.005. This means randomly reversing one bit of the children's DNA with the possibility of M, which is shown in Fig. 6. Usually, the mutation rate is set to be around 0 ~ 0.1

g) Obtaining new population after cross-over and mutation

h) Iterating the step b) to g) for N^{th} generations until the whole populations are gradually converging into one optimal point with the highest fitness value, where 9 generations is required here. If the converging speed is too slow, slightly increase the crossover rate 0.05 will help since it makes the next generation inherit more from the previous generation. If the converging speed is too fast, which might lead to the local optimal solution rather than the global optimal solution, and then the mutation rate should be increased slightly 0.001 to ensure the searching within the whole range

i) Repeating the step a) to h) several times to verify the optimal point obtained in step h). This is to get rid of the local optimal solution due to the limited computation power and parallel processing ability

j) Obtaining the optimal point, which is also the desire design value of the external inductance

Instead of traditional enumeration method which takes all 1024 times of possibilities into consideration, GA provides

directional optimization with only 207 times of simulation, thus accelerating the solution searching process by around 80%.

The methodology of implementing GA into parametric design can be summarized in flowchart shown in Fig. 7.

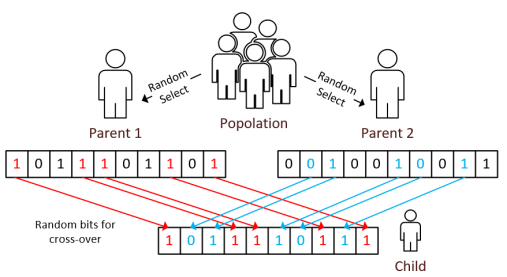

Fig. 5.Cross-over Schematic

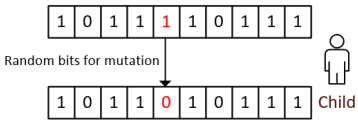

Fig. 6.Mutation Schematic

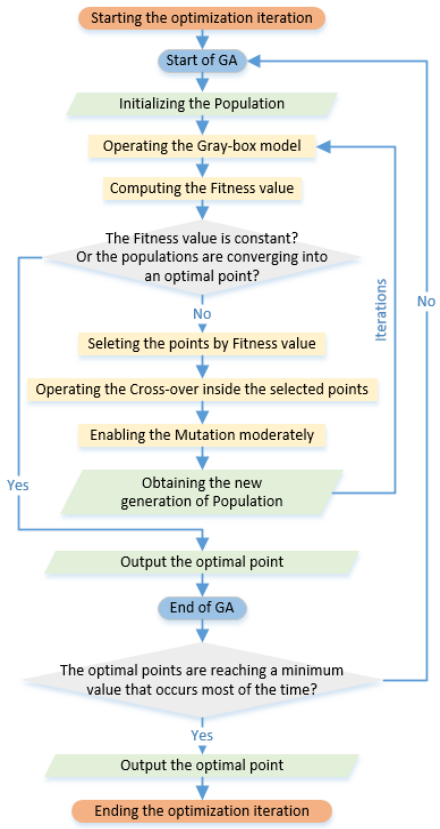

Fig. 7.Flowchart of Implementing GA Methodology

The visualization of the population evolution is shown in Fig. 8, where the X-axis is the HV side external inductance value, Y-axis is the total copper loss of two external inductors, and the red dots stand for the population. It can be observed that, with the iterations of genetic evolution, the randomly distributed population is gradually converging into a single point, which is known as the optimal point, shown as population 9 (Pop9). Several points indicating the excessive copper loss from the findings in population 1 (Pop1) to population 3 (Pop3). Those points are analyzed and compared with the optimal point in the following sections.

The traditional enumeration method is also carried out for comparison, where the visualization of it is shown in Fig. 9. As is observed that, the overall minimum loss is located at around L_{e1} = 0.4μH, which is corresponding to the GA converged result. In addition, several odds points with large loss are observed at certain inductance values. During the evolution process of GA, the odd points are partly captured and eliminated in the next generation. The comparison proves that GA converged to a global optimum rather than local optimum.

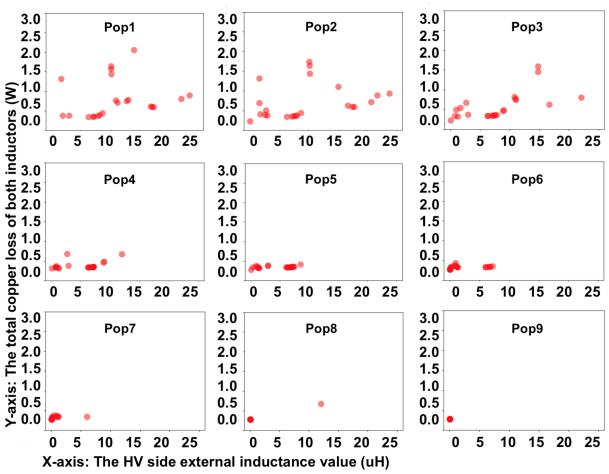

Fig. 8.The Population Evolution Schematic

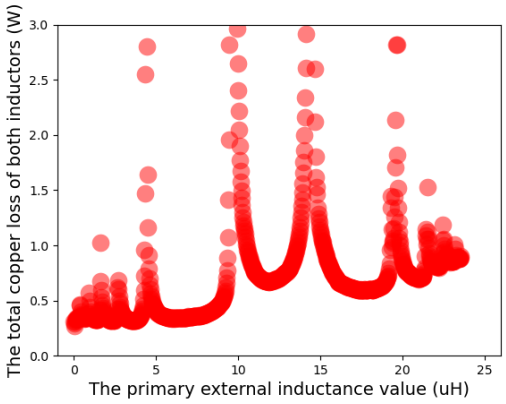

Fig. 9.The Traditional Enumeration Method Schematic

IV. Simulation Result and HFO Analysis

During the GA processing, some points with excessive loss are observed as shown in Fig. 8. When L_{e1} = 10μH and 15μH, the copper loss is large comparing to other points. The minimized copper loss is found when L_{e1} = 0.4μH. The simulated current waveform with L_{e1} = 10μH and 0.4μH are shown in Fig. 10 a) and b) respectively. It can be observed from Fig. 10 a) that there are large harmonic currents passing through the inductor at certain inductance value, which causes detrimental current distortion. Thus, excessive ac loss can be expected. It's found in Fig. 8 that the harmonic amplitude is sensitive to the inductance variance. It can be deduced that the

complex impedance network including parasitics forms a high-order resonant system. Giving certain inductance value together with system parasitic capacitances, the endogenous current harmonic close to the resonant frequency is able to pass through the impedance network, thus distorting the inductor current. The detailed analysis of this high-frequency-oscillation (HFO) is given below.

During the transient period when the S_1 and S_4 turned on, S_2 and S_3 turned off, the interfacing points V_{ac1} rises from -U_{in} to U_{in}. The high frequency excitation voltage is applied on the impedance network seen from V_{ac1}. The frequency spectrum of dv/dt excitation was analyzed in [14]. The waveform of excitation voltage at ac link V_{ac1} is shown in Fig. 11 and can be expressed mathematically in time domain as,

$$V_{\mathrm{ac1}}(\mathrm{t}) = \frac{2U_{\mathrm{in}}}{t_{\mathrm{rise}}}[tu(\mathrm{t}) - (t - t_{\mathrm{rise}})u(t - t_{\mathrm{rise}})] - U_{\mathrm{in}} \quad (17)$$

where the u(t) is a unit step function, U_{in} is the input voltage of the DAB converter, t_{rise} is the rising time. Thus, the Fourier transformation can be adopted for frequency domain analysis,

$$V_{\mathrm{ac1}}(\mathrm{j}\omega) = \frac{2U_{\mathrm{in}}}{\omega^2 t_{\mathrm{rise}}}[\cos(\omega t_{\mathrm{rise}}) - 1 - j\sin(\omega t_{\mathrm{rise}})], \quad (\omega > 0) \quad (18)$$

and corresponding magnitude can be found in Fig. 12.

$$|V_{\mathrm{ac1}}(\mathrm{j}\omega)| = \frac{2U_{\mathrm{in}}}{\omega^2 t_{\mathrm{rise}}}\sqrt{2 - 2\cos(\omega t_{\mathrm{rise}})}, (\omega > 0) \quad (19)$$

The zero crossing points (ZCP) is defined as where the above magnitude reaches zero,

$$\omega = n \cdot 2\pi / t_{\mathrm{rise}}, (n \in N^*) \quad (20)$$

It is obvious that there are no harmonics at the ZCP frequency inside the dv/dt excitation. Thus, it's vital to match the impedance path frequency with the ZCP frequency for no oscillation design. With relatively fast switching speed (high dv/dt ratio), the frequency of ZCP is relatively high. So it's easier to tune the path frequency to the first ZCP frequency in this case.

$$f_{\mathrm{ZCP}} = 1/t_{\mathrm{rise}} \quad (21)$$

The equivalent impedance network seen from the interfacing points V_{ac1} is shown in Fig. 13. and can be expressed mathematically as Z_{in} in (22). It can be derived from the bode plot of Z_{in} that there are two zeros of the impedance network and the first zero is where the low impedance path exists. Thus, the harmonics of the same frequency can pass through the impedance network and cause distortion.

$$Z_{\mathrm{s}} = j\omega L_{\mathrm{k2}} + \frac{\frac{j\omega L_{\mathrm{e2}} + R_{\mathrm{eq}}}{j\omega C_{\mathrm{p2}}}}{j\omega L_{\mathrm{e2}} + R_{\mathrm{eq}} + \frac{1}{j\omega C_{\mathrm{p2}}}}, Z_{\mathrm{seq}} = \frac{N^2 Z_{\mathrm{s}} \cdot j\omega L_{\mathrm{M}}}{N^2 Z_{\mathrm{s}} + j\omega L_{\mathrm{M}}},$$

$$Z_{\mathrm{in}} = j\omega L_{\mathrm{e1}} + \frac{\frac{j\omega L_{\mathrm{k1}} + Z_{\mathrm{seq}}}{j\omega C_{\mathrm{p1}}}}{j\omega L_{\mathrm{k1}} + Z_{\mathrm{seq}} + \frac{1}{j\omega C_{\mathrm{p1}}}} \quad (22)$$

With the traditional DAB converters [23] or symmetrical splitting inductance method [14], the impedance network is nonadjustable with fixed frequency response. However, this asymmetrical splitting inductance method enables the adjustment of impedance network's frequency characteristics by tuning L_{e1} and L_{e2}. With parameters derived from the constructed prototype, the tuning frequency range of the first zero (path frequency) can be obtained shown in Fig. 14. With given ZCP frequency, corresponding inductance value L_{e1} can be determined. Moreover, the fully ZVS range of inductance value L_{e1} can be calculated according to [2] considering proper dead time, which is also marked as the grey area in Fig. 14. It can be observed that the require L_{e1} in this case doesn't fit for fully ZVS operation due to lack of stored energy for discharging the output capacitance of the switches. However, partial ZVS can still be achieved. Arguing that the eliminating HFO contributes more in reducing the EMI and loss while the partial ZVS of switches are acceptable, the choice of L_{e1} mainly relies on ZCP frequency. Note that the analysis is valid for both forward and reverse conditions of bi-directional power flow.

With L_{e1} = 0.4μH referring to the minimal loss according to the GA processed result, the current waveform is shown in Fig. 10 b). Low harmonics and little current distortion can be observed comparing with other waveforms, which is corresponding to the matching of impedance path frequency and ZCP frequency as addressed above. Thus, the L_{e1} = 0.4μH is the optimal point that gives the design guidelines for the following prototype constructing and experiment.

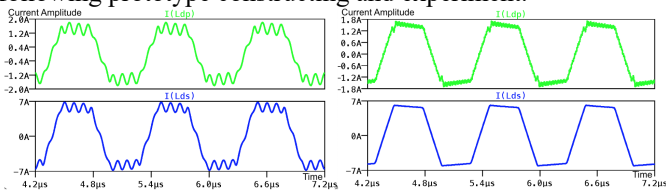

Fig. 10. The Current Waveforms from Simulation

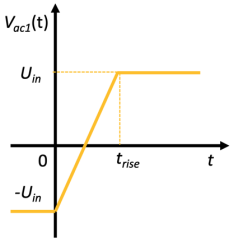

Fig. 11. Excitation Voltage at ac Link

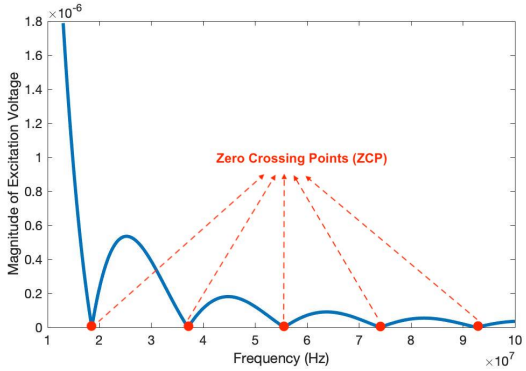

Fig. 12. Excitation Voltage Frequency Spectrum

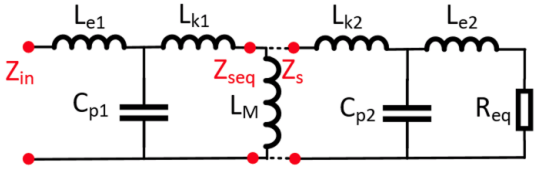

Fig. 13. Equivalent Impedance Network

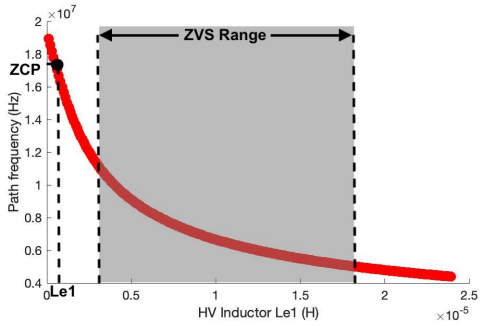

Fig. 14. Path Frequency Range and Fully ZVS Range

V. Experiment Result Analysis

The DAB prototype with 1 MHz operating frequency is built as shown in Fig. 15, where the specifications can be found in TABLE I. Under the SPS modulation, the phase shift of between the primary bridge and secondary bridge is set to be -29π/50 to deliver the required output power.

The rising time t_{rise} is measured by the ac link voltage (switching node voltage), which is 54.2 ns and the first ZCP frequency can be calculated by (21) to be 18.45 MHz. By referring to Fig.5, we can obtain the required HV side inductance value. The L_{e1} = 365 nH, L_{e2} = 1.48 μH are chosen as the optimal set measured by the Agilent 4294A precision impedance analyzer and the L_{e1} = 9.9 μH, L_{e2} = 900 nH are chosen to be the comparing set. It can be seen from the bode plot in Fig. 16 that the first zero frequency of the optimal set is 17.9 MHz and the comparing set is 6.69 MHz. The ZCP frequency is very close to the optimal set path frequency but far away from the comparing set path frequency.

The main waveform of the optimal set and comparing set are shown in Fig. 17 . It can be observed from the high side current HV-I and low side current LV-I that there are nearly zero current oscillation going through the inductors with optimal set, but large high frequency current oscillation on comparing set. The measured oscillation frequency from the experiment is 4.6 MHz which is slightly different from the calculated 6.69 MHz path frequency, the bias mainly comes from the impedance measurement and parasitic derivation. It can be observed from the drain to source voltage of the high voltage side FET HV-Vds that the optimal set are not achieving fully ZVS, thus introducing high frequency spike on top of the trapezoidal current. This might also cause the EMI problem. The partial ZVS condition with optimal set is because of the small inductance value assigned to the HV side inductor. Small HV side inductor stores less energy and requires longer dead time for charging and discharging the HV side FETs, where the detailed ZVS region calculation can be found in [2]. In fact, by tuning the ZCP frequency to be smaller according to Fig. 14, the inductance of optimal set can be placed into the region of achieving fully ZVS. Thus, switches with smaller C_{oss} value are required to operate with shorter rising time according to (21). In order to control variables, the dead time of two sets is set to be equal, which is 40ns in this case.

While keeping other conditions same, the efficiency measurement from the N4L precision power analyzer indicates that the optimal set is operating with 93.4 % efficiency at 186W and the comparing set is operating with 89.5% at 164W. Higher efficiency of the optimal set at even higher power proves the lower loss in the magnetics components laterally. The magnetic thermal image of optimal set and comparing set are shown in Fig. 18. The spot 1 is the HV side inductor and the optimal set temperature is 9 °C lower. The spot 2 is the Transformer and the optimal set temperature is 5.5 °C lower. And the spot 3 is the LV side inductor and the optimal set temperature is 7.5 °C lower. All magnetic components operating with lower power bearing with higher temperature in the comparing set validates that the HFO leads to extra loss. However, due to partial ZVS condition of the optimal set and higher power delivering, the HV side FET are operating with slightly higher temperature than the comparing set achieving fully ZVS, which can be observed in Fig. 19.

With lighter load condition, smaller phase shift is required which causes slight change in the rising time of switching node voltage V_{ac1}. Consequently, slight changes of ZCP frequency are obtained as shown in Fig. 12. While the path frequency of both sets keeps unchanged, the HFO thus can still be observed in comparing set and eliminated in optimal set. The waveforms are similar to the full-load condition as shown in Fig. 17.

With reverse power flow of rated power, similar waveforms are observed as shown in Fig. 20. Same analysis can be applied to the reverse condition regarding the HFO and splitting inductance method. Still, with path frequency of optimal set is closer to first ZCP frequency and path frequency of comparing set is much lower than the first ZCP frequency, the HFO is thus eliminated in optimal set and still observed in comparing set.

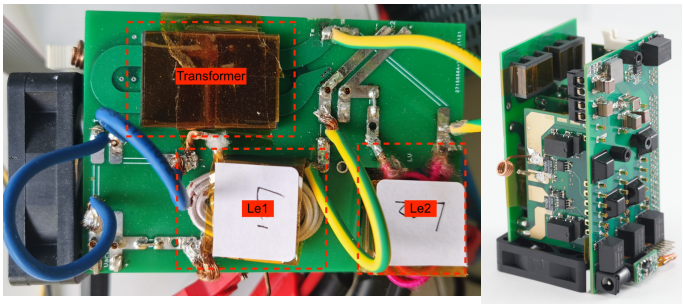

Fig. 15. The Experimental DAB Prototype

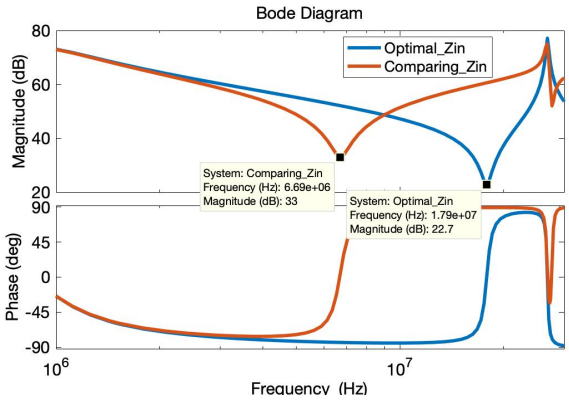

Fig. 16. Input Impedance Bode Plot: Optimal Set /Comparing Set

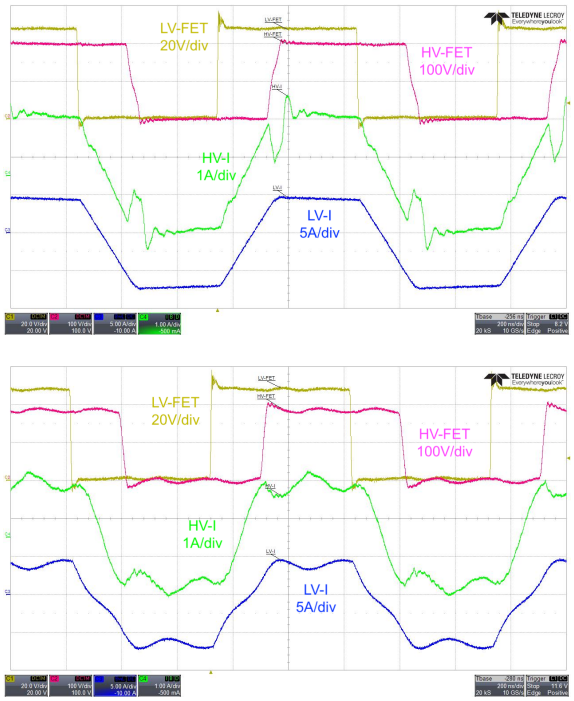

Fig. 17. Waveforms: Top-Optimal Set / Bottom-Comparing Set

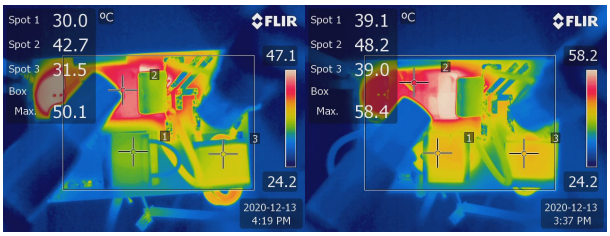

Fig. 18. Magnetic Thermal Images: Optimal Set/ Comparing Set

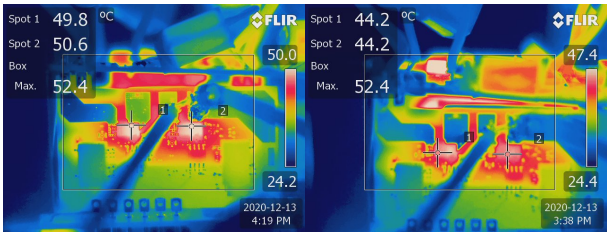

Fig. 19. HV-FET Thermal Images: Optimal Set / Comparing Set

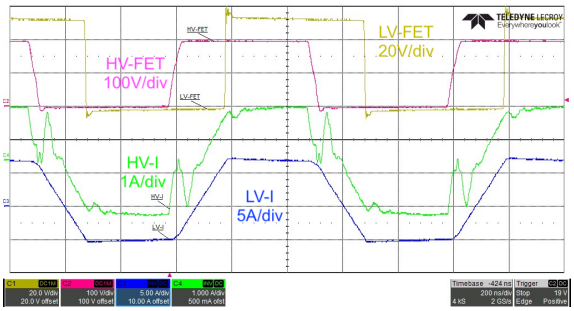

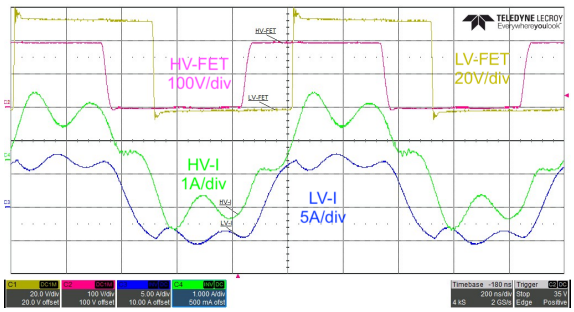

Fig. 20. Reverse Power Flow Waveforms: Top-Optimal Set / Bottom-Comparing Set

VI. CONCLUSIONS

This paper implemented a GA assisted method for parametric design of DAB converter and proposed a splitting inductance tuning method to eliminate the high frequency oscillation problem in DAB converter. The gray-box model of the DAB converter including parasitics, transient coefficient and the thermal effect is described. The GA is implemented to minimize the total conduction loss of both external inductors. The methodology of applying GA into circuit parametrical design is elaborated. The impedance tuning approach is analyzed with the constructed prototype parameters. A 1 MHz GaN-based DAB experiment prototype is built and tested with an optimal set of inductors and a comparing set. The experimental comparison validates the GA approach and proves the feasibility of the proposed splitting inductance tuning method. This work indicates the possibility of combining GA with power electronic design and optimization. Comparing with the traditional analytical design method, GA helps in avoiding the complex theoretical derivation with its strong computing power and enables the circuit analysis with a more realistic model. This indicates the advantage of implementing more advanced algorithms of AI field into more complex power electronics design.

REFERENCES

[1] W. A. A. de Doncker and D. M. Divan, “A Three-phase Soft-Switched High-Power-Density dc/dc Converter for High-Power Applications,” vol. 27, no. 1, 1991.

[2] Y. Xiao, Z. Zhang, M. A. E. Andersen, and K. Sun, “Impact on ZVS Operation by Splitting Inductance to Both Sides of Transformer for 1-MHz GaN Based DAB Converter,” *IEEE Transactions on Power Electronics*, pp. 1–1, 2020, doi: 10.1109/TPEL.2020.2988638.

[3] F. Krismer and J. W. Kolar, “Efficiency-optimized high-current dual active bridge converter for automotive applications,” *IEEE Transactions on Industrial Electronics*, vol. 59, no. 7, pp. 2745–2760, Jul. 2012, doi: 10.1109/TIE.2011.2112312.

[4] C. Wang, M. Li, Z. Ouyang, and G. Wang, “Resonant Push-pull Converter with Flyback Regulator for MHz High Step-Up Power Conversion,” *IEEE Transactions on Industrial Electronics*, pp. 1–1, 2020, doi: 10.1109/TIE.2020.2969109.

[5] Y. Wang, O. Lucia, Z. Zhang, S. Gao, Y. Guan, and D. Xu, “A Review of High Frequency Power Converters and Related Technologies,” *IEEE Open Journal of the Industrial Electronics Society*, vol. 1, pp. 247–260, Sep. 2020, doi: 10.1109/ojies.2020.3023691.

[6] Y. Yan, H. Gui, and H. Bai, "Complete ZVS Analysis in Dual-Active-Bridge," *IEEE Transactions on Power Electronics*, vol. 8993, no. c, pp. 1–1, 2020, doi: 10.1109/tpel.2020.3011470.

[7] Z. Qin, Z. Shen, and F. Blaabjerg, "Modelling and analysis of the transformer current resonance in dual active bridge converters," in *2017 IEEE Energy Conversion Congress and Exposition (ECCE)*, Oct. 2017, pp. 4520–4524, doi: 10.1109/ECCE.2017.8096775.

[8] S. Zhao, F. Blaabjerg, and H. Wang, "An Overview of Artificial Intelligence Applications for Power Electronics," *IEEE Transactions on Power Electronics*, pp. 1–1, 2020, doi: 10.1109/tpel.2020.3024914.

[9] M. Liserre, A. Dell'Aquila, and F. Blaabjerg, "Genetic algorithm-based design of the active damping for an LCL-filter three-phase active rectifier," *IEEE Transactions on Power Electronics*, vol. 19, no. 1, pp. 76–86, 2004, doi: 10.1109/TPEL.2003.820540.

[10] A. Garcia-Bediaga, I. Villar, A. Rujas, L. Mir, and A. Rufer, "Multiobjective optimization of medium-frequency transformers for isolated soft-switching converters using a genetic algorithm," in *IEEE Transactions on Power Electronics*, Apr. 2017, vol. 32, no. 4, pp. 2995–3006, doi: 10.1109/TPEL.2016.2574499.

[11] B. Zhao, X. Zhang, and J. Huang, "AI algorithm-based two-stage optimal design methodology of high-efficiency CLLC resonant converters for the hybrid AC-DC microgrid applications," *IEEE Transactions on Industrial Electronics*, vol. 66, no. 12, pp. 9756–9767, Dec. 2019, doi: 10.1109/TIE.2019.2896235.

[12] K. Ishaque and Z. Salam, "A deterministic particle swarm optimization maximum power point tracker for photovoltaic system under partial shading condition," *IEEE Transactions on Industrial Electronics*, vol. 60, no. 8, pp. 3195–3206, 2013, doi: 10.1109/TIE.2012.2200223.

[13] T. Dragicevic, P. Wheeler, and F. Blaabjerg, "Artificial Intelligence Aided Automated Design for Reliability of Power Electronic Systems," *IEEE Transactions on Power Electronics*, vol. 34, no. 8, pp. 7161–7171, Aug. 2019, doi: 10.1109/TPEL.2018.2883947.

[14] B. Cui, P. Xue, and X. Jiang, "Elimination of High Frequency Oscillation in Dual Active Bridge Converters by dv / dt Optimization," *IEEE Access*, vol. 7, pp. 55554–55564, 2019, doi: 10.1109/ACCESS.2019.2910597.

[15] H. Bai, Z. Nie, and C. C. Mi, "Experimental comparison of traditional phase-shift, dual-phase-shift, and model-based control of isolated bidirectional dc-dc converters," *IEEE Transactions on Power Electronics*, vol. 25, no. 6, pp. 1444–1449, 2010, doi: 10.1109/TPEL.2009.2039648.

[16] F. Krismer and J. W. Kolar, "Accurate small-signal model for the digital control of an automotive bidirectional dual active bridge," *IEEE Transactions on Power Electronics*, vol. 24, no. 12, pp. 2756–2768, 2009, doi: 10.1109/TPEL.2009.2027904.

[17] H. Qin and J. W. Kimball, "Generalized average modeling of dual active bridge DC-DC converter," *IEEE Transactions on Power Electronics*, vol. 27, no. 4, pp. 2078–2084, 2012, doi: 10.1109/TPEL.2011.2165734.

[18] F. Krismer and J. W. Kolar, "Accurate power loss model derivation of a high-current dual active bridge converter for an automotive application," *IEEE Transactions on Industrial Electronics*, vol. 57, no. 3, pp. 881–891, 2010, doi: 10.1109/TIE.2009.2025284.

[19] C. Galup-Montoro and M.´Rcio C. Schneider, *MOSFET Modeling for Circuit Analysis and Design*. 2007.

[20] R. Beach and A. (Epc Corp.) Babakhani, "Circuit Simulation Using EPC Device Models," *Application Notes*, 2010. .

[21] K. de Jong, "Adaptive system design: A Genetic Approach," *IEEE Transactions on Systems, Man and Cybernetics*, no. 9, pp. 566–574, 1980.

[22] R. Leardi, "Optimization of Control Parameters for Genetic Algorithms," *Comprehensive Chemometrics*, vol. 1, no. February, pp. 631–653, 2009, doi: 10.1016/B978-044452701-1.00039-9.

[23] W. Song, N. Hou, and M. Wu, "Virtual Direct Power Control Scheme of Dual Active Bridge DC-DC Converters for Fast Dynamic Response," *IEEE Transactions on Power Electronics*, vol. 33, no. 2, pp. 1750–1759, Feb. 2018, doi: 10.1109/TPEL.2017.2682982.

Chang Wang was born in Wuhan, China, in 1994. He received the B.S.E degree in measurement control technology and instruments from Shanghai Jiao Tong University (SJTU), Shanghai, China, in 2017, and the M.Sc. degree in power electronics from Technical University of Denmark (DTU), Kongens Lyngby, Denmark, in 2019.

He is currently a Ph.D. student working towards advanced power electronics with artificial intelligence in Department of Electrical Engineering, Technical University of Denmark. His research interests include high-density high-efficiency bi-directional dc-dc converters, high-frequency planar magnetics, wireless charging and artificial intelligence implementation in power electronics.

Tiberiu-Gabriel Zsurzsan received his B.Sc. degree in Applied Electronics from the Polytechnic University of Timisoara, Romania, in 2010 and his M.Sc. degree in Automation and Robotics from the Technical University of Denmark, Kongens Lyngby, Denmark, in 2012 and his Ph.D. degree from the Technical University of Denmark in 2016. He is currently an assistant professor at the same university and his main research interests include sensing and sensor systems, human motion tracking, harsh environment electronics, modelling and control of exotic motors as well as piezoelectric vibrations.

Zhe Zhang (Senior Member, IEEE) received the B.Sc. and M.Sc. degrees in power electronics from Yanshan University, Qinhuangdao, China, in 2002 and 2005, respectively, and the Ph.D. degree in electrical engineering from the Technical University of Denmark, Kongens Lyngby, Denmark, in 2010. He is currently an Associate Professor with the Department of Electrical Engineering, Technical University of Denmark (DTU). Since January 2018, he has been the Head of Studies in charge of Electrical Engineering M.Sc. Programme at DTU. From 2005 to 2007, he was an Assistant Professor with Yanshan University. From June 2010 to August 2010, he was with the University of California, Irvine, CA, USA, as a Visiting Scholar. He was an Assistant Professor with the Technical University of Denmark, from 2011 to 2014. He has authored or co-authored more than 150 transactions and international conference papers and filed over ten patent applications. He has supervised more than ten Ph.D. students since 2013. His current research interests include applications of wide bandgap devices, high frequency dc–dc converters, multiple-input dc–dc converters, softswitching power converters, and multilevel dc–ac inverters for renewable energy systems, hybrid electric vehicles and uninterruptable power supplies; piezoelectric-actuator and piezoelectric-transformer based power conversion systems. Dr. Zhang was the recipient of several awards and honors including Best Paper Awards in IEEE ECCE 2016, IEEE IGBSG 2018, IEEE IFEEC 2019, IEEE ECCE Asia 2020, Best Teacher of the Semester, Chinese Government Award for Outstanding Students Abroad, etc. He is also an Associate Editor for IEEE TRANSACTIONS ON INDUSTRIAL ELECTRONICS, Associate Editor for IEEE JOURNAL OF EMERGING AND SELECTED TOPICS IN POWER ELECTRONICS, Associate Editor for IEEE ACCESS, and Guest Editor for IEEE JOURNAL OF EMERGING AND SELECTED TOPICS IN INDUSTRIAL ELECTRONICS.